BNL-209062-2018-JAAM

Temperature-Dependent Kinetics and Reaction Mechanism of Ammonia Oxidation on Pt, Ir, and PtIr Alloy Catalysts

L. Song, J. X. Wang

To be published in "Journal of Electrochemical Society "

September 2018

Chemistry Department

Brookhaven National Laboratory

U.S. Department of Energy

USDOE Office of Science (SC), Basic Energy Sciences (BES) (SC-22)

DISCLAIMER

Temperature-Dependent Kinetics and Reaction Mechanism of Ammonia Oxidation on Pt, Ir, and PtIr Alloy Catalysts

Liang Song,[1] Zhixiu Liang, [1] Zhong Ma,[1] Yu Zhang,[1] Jingyi Chen,[2] Radoslav R. Adzic,[1]

and Jia X. Wang[1]

[1]Brookhaven National Laboratory, Chemistry Division, Energy & Photon Sciences Directorate, Upton, NY 11973, USA

[2]University of Arkansas, Department of Chemistry and Biochemistry, 345 N. Campus Drive Fayetteville, AR 72701, USA

ABSTRACT

We report here a kinetic study of ammonia oxidation reaction (AOR) on carbon supported Pt, Ir, and PtIr (1:1) alloy catalysts using gas diffusion electrodes in 1 M KOH solution at temperatures up to 60 ^{o}C. Ammonia concentration was kept constant by letting Ar gas bubbling through concentrated ammonia solution before entering the cell. At 0.5 V versus reversible hydrogen electrode, the currents normalized to the mass of platinum group metals are in the order of PtIr > Ir > Pt. Compared to Pt, Ir exhibited higher activity enhancement with increasing temperature, lower onset potential, and lower peak current. In correlation with previous theoretical studies, these differences are ascribed to Ir having lower activation barrier for the first one-electron deprotonation of NH_3 to NH_2*, but higher barrier for dimerization of two NH_2* to N_2H_4*. The AOR current peaks at high potentials because the rate is limited by the potential-independent dimerization and formation of inactive N* that blocks the active surface. Below peak potentials, gradual deactivation occurs due to the accumulation of NH* that is harder to be dimerized than NH_2*. PtIr alloy combines the virtues of Ir and Pt exhibiting the widest active potential window and the highest peak current.

Direct ammonia fuel cells (DAFC) is an attractive alternative of hydrogen fuel cells because ammonia is a carbon-free hydrogen carrier with a specific energy density 50% higher than liquefied hydrogen.[1] It was less studied than other liquid fuels, such as, methanol and ethanol, partly because ammonia oxidation reaction (AOR) operates in alkaline media, not suitable for proton exchange membrane fuel cells. Recent advances in developing alkaline membrane fuel cells[2–5] stimulated the interest in DAFC. Over the last decade, the peak power density of hydrogen alkaline fuel cells increased tenfold from 130 to 1400 mW cm^{-2}, resulting mainly from ongoing progress in enhancing the anion conductivity of hydroxide membranes.[5] A major remaining challenge is the need for more active and durable anode catalysts for various fuels, including hydrogen.[6] This is because hydrogen oxidation reaction (HOR) rate on platinum group metals (PGM) is lower in base than in acid by two orders of magnitude.[7,8] Thus, it is particularly significant if high performance, low-PGM catalysts can be developed for oxidation of liquid fuels in base.

In the classic DAFC studies carried out in 1969,[9,10] significant AOR activities were demonstrated at elevated temperatures using Pt, Ir and PtIr alloy particles. At 140 °C, anode overpotentials of 0.22 and 0.23 V at 0.2 A cm^{-2} were demonstrated using Ir and PtIr, respectively, albeit with high metal loadings of 34 mg cm^{-2}. Lowering temperature from 140 to 80 and 25 °C caused the overpotential at an Ir anode increased from 0.23 to 0.33 and 0.50 V, respectively. These results demonstrated encouragingly low anode overpotentials of DAFC at elevated temperatures and the need for developing more active, low-PGM-content catalysts for AOR.

Pt has been studied mostly since it yields the highest AOR peak current and Ir is known for its lowest onset potential.[11–15,16] Thus, Pt, Ir, and PtIr alloy nanocatalysts are the baseline materials for AOR studies.[17,18] Quantitative comparison of AOR catalysts remains elusive because

the data accumulated so far were obtained using various potential sweep rates, ammonia concentrations, pH values, and were not normalized to PGM loadings.[19] Effort for making AOR performance more generally comparable has started as a recent study investigated the effect of these experimental parameters on the AOR polarization curves measured for Pt/C, Ir/C and Rh/C.[20]

Here, we report a temperature-dependent AOR kinetic study of carbon-supported Pt, Ir, and PtIr catalysts with the ammonia concentration kept at the saturation with ammonia vapor in an inert gas flow. The measurement method and temperature-dependent AOR polarization curves from 25 to 60 ^{o}C are presented using the results for the PtIr catalyst. At 60 ^{o}C, AOR currents increase significantly below 0.6 V versus reversible hydrogen electrode (RHE), which is the most relevant potential region for DAFC. For the Pt and Ir catalysts, we correlate measured onset potentials, peak currents, and temperature enhancement factors to previously published theoretical results, which is briefly description in the next section. The currents normalized to PGM mass at 0.5 V is used for comparing the performance of three AOR catalysts. The last topic is an investigation of the cause of deactivation within the potential window for AOR between the onset and peak potentials.

Theoretical Background

Compared to the two-electron (2e) oxidation of hydrogen, the 6e AOR, $2NH_3 + 6OH^- = N_2 + 6H_2O + 6e^-$, produces N_2 in addition of H_2O. The generally accepted reaction scheme involves a dimerization step without electron transfer for the N-N bond formation,

$NH_x^* + NH_y^* = H_xN\text{-}NH_y^*$,

where x and y can be 2, 1, and 0; * indicates an adsorbed reaction intermediate. All deprotonation steps, either before or after dimerization, involve single electron transfer. i.e.,

$$NH_x^* + OH^- = NH_{x-1}^* + H_2O + e^-$$

or $N_2H_{(x+y)}^* + OH^- = N_2H_{(x+y-1)}^* + H_2O + e^-$.

Thus, the values of x and y determine the reaction pathways. The N*-N* or N_2 dimerization pathway was suggested by Oswin and Salomon in 1963.[21] In 1970, Gerischer and Mauerer proposed reaction pathways via $NH_x^* + NH_y^*$ dimerization with x and y being 2 or 1.[22] A density functional theory (DFT) study carried out by Herron, Ferrin and Mavrikakis in 2015 verified that the Gerischer-Mauerer mechanism is kinetically preferred on Pt and Ir and that inactive N* poisons the catalyst surface,[23] which is consistent with the conclusions of many experimental studies.[14,24–27] A remaining question is whether dimerization pathways involving NH* are active on Pt and Ir.[27]

Based on DFT calculated activation energies, E_a, for dimerization steps and reaction free energies, ΔG, for the 1e deprotonation steps reported in the abovementioned reference,[23] the three lowest activation barriers for dimerization are for the pathways involving at least one NH_2*. Figure 1 shows these reaction pathways and the calculated E_a and ΔG values for Pt and Ir. In both cases, as the green arrows indicated, the active AOR pathway is *via* H_2N^*-NH_2^* dimerization that has the lowest activation energy, E_a. The second lowest E_a is for N* + NH_2*, and the third lowest is for NH* + NH_2*. Interestingly, the E_a for dimerizing NH* (1.52 eV for Pt and 1.51 eV for Ir) is much higher than those for dimerizing N* (1.21 eV for Pt and 1.29 eV for Ir). Thus, NH* is highly inactive for dimerization, but can be deprotonated to N* at high potentials. These results suggest that the hydrazine pathway, i.e., dimerization of two NH_2* to form N_2H_4*, is the active pathway for Pt and Ir.

For the 1e deprotonation steps, the reaction free energies were used to be approximately as the minimum potentials for the reactions to occur,[23] and can also be considered as the minimal values for activation energy. We used shorter horizontal arrows for the lower ΔG values to represent faster reaction rates. Thus, the long green arrows indicate the rate-limiting steps for deprotonation in the active H_2N^*-NH_2^* dimerization pathway, which differ for Pt and Ir.

While our focus of this study is on the material characterization and comparing experimental results of the trend for polycrystalline nanoparticles with theoretical results, it is worth to note that AOR is a facet sensitive reaction. Studies on Pt single crystals in 1 mM ammonia solution have shown that the onset potential can vary from 460 mV on (111) to 560 mV on (210) surface and the peak current can differ by 33 times from 20 μA cm^{-2} on (111) to 660 μA cm^{-2} on (100). There is a gap between polycrystalline surface of experimental materials and (111) surface model used in the DFT calculations. However, the material trend seems to be independent of facets, e. g., compared to Pt(100), Ir(100) exhibited lower onset potential and lower peak current,[28] similar to that for Pt/C and Ir/C.[20]

Experimental

Catalyst inks were made by dispersing Ir/C, Pt/C, and IrPt/C (Premetek, 40 wt% metal, Ir:Pt molar ratio 1:1) in mixed solvent of deionized water, ethanol, and isopropanol (volume ratio 1:1:2). Nafion® (perfluorinated resin, equivalent weight 1000, Aldrich) was added as a binder to stabilize catalyst layer. The ionomer to carbon weight ratio was 0.3 to 0.5. The gas diffusion layer (Sigracet 25 BC) was cut into 1.4 cm wide and 3 cm long strips for making gas diffusion electrode (GDE) samples. Catalyst ink of 12.5 μL containing 0.1 mg metal is drop casted on $1.4 \times 0.7 = 1$ cm^2 area at one end of the GDL strips. After drying in air, the catalyst-loading samples were immersed in 1

M KOH to deacidify Nafion ionomer before measurements in alkaline solutions. The measured currents were normalized to the PGM loading of 0.1 mg and thus was not affected by small variation of catalyst coating area. Results shown represent the average performance of four or more samples.

Electrochemical measurements were performed using a Voltalab PGZ 402 potentiostat with an electrochemical cell immersed in a water bath with temperature control (Lauda E100). We held a GDE strip vertically with its catalyst-coated part immersed in solution and faced a Pt-flag counter electrode that was about 1 cm away. A Hg/HgO electrode was used as the reference electrode. The zero potential versus reversible hydrogen electrode (RHE) in 1 M KOH was determined by the open circuit potential on Pt in hydrogen saturated solution. We recorded cyclic voltammetry curves after purging the 1 M KOH electrolyte with argon. The AOR polarization curves were measured in 1 M KOH solution with argon gas bubbling through 30% NH_4OH solution before entering the cell for keeping the solution oxygen free and ammonia saturated with constant NH_3 vapor. Figure 2 shows the bubbler and electrochemical cell. The iR-free potential was obtained by subtracting the product of measured currents and the high-frequency resistance determined from electrochemical impedance spectra acquired at 500 mV versus RHE.

Results and Discussion

Stabilizing ammonia concentration. - Initially, we measured AOR polarization curves in a 1 M KOH solution containing 0.1 M ammonia at 60 °C. As shown in Figure 3a, considerable current decay was observed after one hour at open circuit. This is attributed to the decrease of ammonia concentration due to ammonia vapor leaking out of the cell when Ar gas is flowing in the cell to keep solution oxygen free. The third curve (red) was taken after letting argon gas bubble through concentrated ammonia solution before entering the electrochemical cell, which exhibited

slightly higher currents than the first curve. This experiment showed the need to stabilize ammonia concentration in a conventional electrochemical cell during AOR measurements at elevated temperatures.

To confirm reproducibility of AOR polarization curves with Ar-NH_3-vapor feeding method, we started with a cell containing 1 M KOH without ammonia. After taking voltammetry curves in deaerated solution, we switched the Ar flow to pass a bubbler containing 30% NH_4OH while running repeated potential cycles within a low potential region. The AOR current rose and reached a stable value about 30 minutes. We then made four potential cycles at 20, 5, 1, and 20 mV s^{-1} sweep rates. As shown in Figure 3b, the first and fourth curves at the same 20 mV s^{-1} sweep rate overlapped well, demonstrating no ammonia concentration variation with time. The other two curves measured at lower sweep rate showed lower currents, which are the AOR kinetic behavior consistent with observations of previous AOR studies at ambient temperature.[20]

Alternatively, pure ammonia gas from a cylinder may be used just like measuring polarization curves for HOR and ORR with pure hydrogen and oxygen, respectively. However, leaking out considerable amount of ammonia from unsealed solution cell would be a practical concern. Therefore, using a bubbler containing about 30 mL concentrated NH_4OH for 4 - 6 hours of AOR measurements is a more suitable method for studying AOR kinetics in solution electrochemical cells.

Effect of high potential limit and temperature-dependent PGM activities. - In a typical measurement of AOR polarization curves, potential cycles starting at 0.05 V were made with increasing high potential limit. Figure 4a shows the results for a PtIr/C sample measured at 60 °C. The first three curves have the curves overlapped in the positive potential sweeps and the currents

in the reversed potential sweeps lowered with higher potential limits. Once the potential went over the peak potential of 0.65 V, severe deactivation occurred. Lowered peak currents obtained from following cycles show that the AOR activity did not fully recover from previous potential cycles. This behavior is commonly observed for the AOR catalysts and has been attributed to the formation of fully deprotonated N* intermediate at high potentials because N* is inactive for dimerization and blocks the surface sites.[16,18,20,27]

To show the temperature effect on AOR peak current, the last potential cycles measured at 25, 40, 50, and 60 °C are shown in Figure 4b. With increasing temperature from 25 to 60 °C, the AOR current increased, especially at low potentials, resulting in lowered onset potentials with the peak current increased about sevenfold. Higher temperature enhancement factor would be expected if only one potential cycle was measured at each temperature to minimize deactivation that was not fully recovered. The curves also show a slight negative shift of the peak potential with rising temperature, which suggests that N* remains inactive and its formation occurs at less positive potential as temperature rises. Thus, the potential window between the onset and current peak only increased slightly. The middle of the potential window is about 0.5 V, suitable for comparing PGM activities of AOR catalysts.

Figure 4c plots the averaged currents of forward and backward potential sweeps measured with the potential cycle to 0.6 V, in which the double layer charging currents are canceled out. Using this method, the currents at 0.5 V show that the AOR activity increased from 18 to 160 A g^{-1}_{PGM}, a factor of nine, as temperature increased from 25 to 60 °C. Both potential sweep rate and high potential limit of the cycle affect the results. The latter is due to the currents in the backward potential sweeps lowers with increasing the high potential limit as shown in Figure 4a.

Comparison of AOR kinetics on Pt/C, Ir/C and PtIr/C.- Using the same potential cycling protocols described above, we plotted selected AOR polarization curves for the three carbon-support catalysts. Figures 5a and 5b show the AOR polarization curves for the Pt, Ir, and PtIr alloy catalysts at 25 and 60 ^{o}C, respectively. Figure 5c shows the voltammetry curves measured at 25 ^{o}C. The three catalysts have similar particle size as determined from XRD peak width. The electrochemical surface areas determined from the hydrogen desorption charge differ within 10%. Thus, the results of mass normalized polarization curves are used for discussion of the material trend for the three catalysts.

The AOR onset potentials are about 0.1 V lower for Ir than Pt at both temperatures. The difference can be explained by the calculated reaction free energies for the first 1e deprotonation of NH_3. While this reaction is exergonic on Ir (i.e., ΔG = -0.1 eV < 0), the reaction free energy on Pt amounts to 0.28 eV (see Figure 1). In addition, the hydrogen desorption current vanishes at a lower potential on Ir than on Pt as shown in Figure 5c, which appears in favor for a lower AOR onset potential on Ir. Above the peak potential, the cause of deactivation can be ascribed to the formation of inactive N* that blocks the surface sites. Compared to Pt, Ir has lower barriers for deprotonation steps toward N* and higher barrier for its dimerization with NH_2* (See Figure 1). Thus, the deactivation occurs on Ir at a lower potential with a lower peak current than on Pt.

Another finding by comparing Figures 5a and 5b is a significantly higher activity enhancement for Ir than Pt with increasing temperature. At 25 ^{o}C, the peak current of Ir is only 23% that of Pt, but the ratio increases substantially to 62% at 60 ^{o}C. In other words, the temperature enhancement factor is higher for Ir than Pt (5.5 versus 2.0). This result rationalizes the better DAFC performance obtained with Ir than Pt at above 100 ^{o}C,[10] while Pt is considered most active based on the studies at ambient temperature in solutions[16,20] and at 40 ^{o}C in DAFC.[18] Since a higher

temperature enhancement is expected for the reaction with higher activation barriers at the rate-limiting steps, we can ascribe Ir's higher temperature enhancement factor to its E_a for dimerization being higher than that of Pt (1.21 versus 1.07 eV) and also the maximum ΔG in the deprotonation steps for Ir and Pt being 0.32 eV > 0.28 eV.

For comparing the performance of AOR catalysts, we note that the PGM mass normalized currents at 0.5 V are in the order of PtIr > Ir > Pt at both temperatures, while the orders for the peak currents change with temperature. As the trend measured by the currents at 0.5 V is consistent with the better performance of PtIr and Ir than Pt at 120 and 140 °C in DAFC and that peak potential can be out of the anode potential range for DAFC, the currents at 0.5 V is more suitable for evaluation of AOR catalysts. The ranking of PtIr (180) > Ir (110) > Pt (20) in unit of A g^{-1}_{PGM} measured at 60 °C emphasizes the importance of enhancing low potential performance for developing advanced AOR catalysts.

Cause of deactivation within the AOR potential window. – As a common behavior of AOR catalysts, currents over the potential window from onset to peak decrease with slower potential sweep rate. We investigate the sustainability of AOR activity using chronoamperometry and chronopotentiometry. Figure 6a shows that the AOR current on a PtIr sample measured at 450 mV decreased by half in 30 minutes (blue curve), and the potential at a constant current of 50 A g^{-1} rose by 65 mV. While these are rather rapid loss in activity, the catalyst is considered structurally stable because about 2/3 of activity loss is recovered in the following AOR polarization curves as shown in Figure 6b. Complete recovery can be made by potential cycles into the hydrogen evolution region.

Distinctly different from the quick vanish of AOR activity during potential sweep at high potentials, the less severe and more recoverable deactivation at low potentials is likely caused by the accumulation of NH* intermediate. As shown in Figure 1, the reaction free energies are low for NH_2* deprotonation to NH* (0.17 eV for Pt and -0.09 eV for Ir), but high for further deprotonation to N* (0.52 eV for Pt and 0.50 eV for Ir). However, NH_2* + NH* dimerization is much harder than dimerization of two NH_2* (0.45 and 0.3 eV higher E_a for Pt and Ir, respectively). Therefore, at potential below where N* forms, the NH* coverage increases with time, which slows down the dimerization and thus the overall reaction rate.

Conclusions

A temperature-dependent kinetic study was carried out for AOR on carbon supported Pt, Ir, and PtIr catalysts with the ammonia concentration kept at saturation by an Ar-NH_3-vapor gas flow. Raising temperature from 25 to 60 ^oC lowers the AOR onset potential and increases the currents within the potential window from the onset to the peak potentials. The current peak ratios for 60 versus 25 ^oC are composition dependent decreasing in the order Ir (5.5) > PtIr (4.2) > Pt (2.0). At 0.5 V, the PGM mass activities are in the order of PtIr > Ir > Pt at both 25 and 60 ^oC. Further increasing temperature may make Ir activity comparable or exceed PtIr due to its temperature enhancement factor being higher than that of PtIr, which is consistent with the previous DAFC results at >100 ^oC.

The common feature of AOR polarization curves for all three catalysts supports the reaction mechanism with the dimerization of two NH_2* to N_2H_4* as the sole active pathway. While inactive N* has been commonly recognized as the cause for AOR current peaks around 0.6 V, NH* is identified in this study as an inactive intermediate at low potentials resulting in a gradual

decay of the AOR activity within the AOR potential window between the onset and peak potentials.

Ir exhibits lower onset potential and lower peak current than Pt due to the activation barriers of Ir being lower for the first 1e deprotonation of NH_3 to NH_2*, but higher for the dimerization of two NH_2* to N_2H_4*. Higher temperature enhancement for AOR on Ir than Pt is consistent with DFT calculated activation barriers in the rate-limiting steps being higher for Ir than Pt. Encouragingly, PtIr alloy combines the virtues of Ir and Pt in boosting the AOR performance - an onset potential as low as Ir and a peak current exceeding that of Pt.

Acknowledgement

This research was funded by the Advanced Research Projects Agency-Energy (ARPA-E), U.S. Department of Energy, under Award Number DE-AR0000805 and by the Division of Chemical Sciences, Geosciences and Biosciences Division, US Department of Energy under contract DE-SC0012704. J.C. acknowledges financial support from the National Science Foundation under Grant No. 1703827.

References

1. F. Vitse, M. Cooper, and G. G. Botte, *J. Power Sources*, **142**, 18–26 (2005).

2. G. Merle, M. Wessling, and K. Nijmeijer, *J. Memb. Sci.*, **377**, 1–35 (2011).

3. S. Gottesfeld et al., *J. Power Sources*, **375**, 170–184 (2018) https://doi.org/10.1016/j.jpowsour.2017.08.010.

4. A. Serov, I. V. Zenyuk, C. G. Arges, and M. Chatenet, *J. Power Sources*, **375**, 149–157 (2018).

5. D. R. Dekel, *J. Power Sources*, **375**, 158–169 (2018) https://doi.org/10.1016/j.jpowsour.2017.07.117.

6. Y. Cong, B. Yi, and Y. Song, *Nano Energy*, **44**, 288–303 (2018) https://doi.org/10.1016/j.nanoen.2017.12.008.

7. W. Sheng, H. A. Gasteiger, and Y. Shao-Horn, *J. Electrochem. Soc.*, **157**, B1529–B1536 (2010) http://jes.ecsdl.org/cgi/doi/10.1149/1.3483106.

8. K. Elbert et al., *ACS Catal.*, **5**, 6764–6772 (2015) http://pubsdc3.acs.org/doi/10.1021/acscatal.5b01670.

9. E. L. Simons, E. J. Cairns, and D. J. Surd, *J. Electrochem. Soc.*, **116**, 556 (1969).

10. D. W. McKee, a. J. Scarpellino, I. F. Danzig, and M. S. Pak, *J. Electrochem. Soc.*, **116**, 562 (1969) http://jes.ecsdl.org/cgi/doi/10.1149/1.2411963.

11. F. J. Vidal-Iglesias, N. Garcia-Araez, V. Montiel, J. M. Feliu, and A. Aldaz, *Electrochem. commun.*, **5**, 22–26 (2003).

12. F. J. Vidal-Iglesias et al., *Electrochem. commun.*, **6**, 1080–1084 (2004).

13. F. J. Vidal-Iglesias, J. Solla-Gullón, V. Montiel, J. M. Feliu, and A. Aldaz, *J. Phys. Chem. B*, **109**, 12914–12919 (2005).

14. F. J. Vidal-Iglesias, J. Solla-Gullón, J. M. Feliu, H. Baltruschat, and A. Aldaz, *J. Electroanal. Chem.*, **588**, 331–338 (2006).

15. R. Acevedo et al., *Microgravity Sci. Technol.*, **29**, 253–261 (2017).

16. F. J. Vidal-Iglesias, J. Solla-Gullón, V. Montiel, J. M. Feliu, and A. Aldaz, *J. Power Sources*, **171**, 448–456 (2007).

17. B. K. Boggs and G. G. Botte, *Electrochim. Acta*, **55**, 5287–5293 (2010) http://dx.doi.org/10.1016/j.electacta.2010.04.040.

18. M. H. M. T. Assumpção et al., *Int. J. Hydrogen Energy*, **39**, 5148–5152 (2014).

19. J. Jiang, *Electrochem. commun.*, **75**, 52–55 (2017) http://dx.doi.org/10.1016/j.elecom.2016.12.017.

20. Z.-F. Li, Y. Wang, and G. G. Botte, *Electrochim. Acta*, **228**, 351–360 (2017) http://linkinghub.elsevier.com/retrieve/pii/S0013468617300208.

21. H. G. Oswin and M. Salomon, *Can. J. Chem.*, **41**, 1686–1694 (1963).

22. H. Gerischer and A. Mauerer, *J. Electroanal. Chem.*, **25**, 421–433 (1970).

23. A. Herron et al., *J. Phys. Chem. C*, **119**, 14692–14701 (2015).

24. N. J. Bunce and D. Bejan, *Electrochim. Acta*, **56**, 8085–8093 (2011) http://dx.doi.org/10.1016/j.electacta.2011.07.078.

25. C. Zhong, W. B. Hu, and Y. F. Cheng, *J. Mater. Chem. A*, **1**, 3216 (2013) http://xlink.rsc.org/?DOI=c2ta00607c.

26. L. A. Diaz and G. G. Botte, *Electrochim. Acta*, **179**, 519–528 (2015) http://dx.doi.org/10.1016/j.electacta.2014.12.162.

27. A. C. A. De Vooys, M. T. M. Koper, R. A. Van Santen, and J. A. R. Van Veen, *J. Electroanal. Chem.*, **506**, 127–137 (2001).

28. N. Sacré et al., *ACS Catal.*, **8**, 2508–2518 (2018).

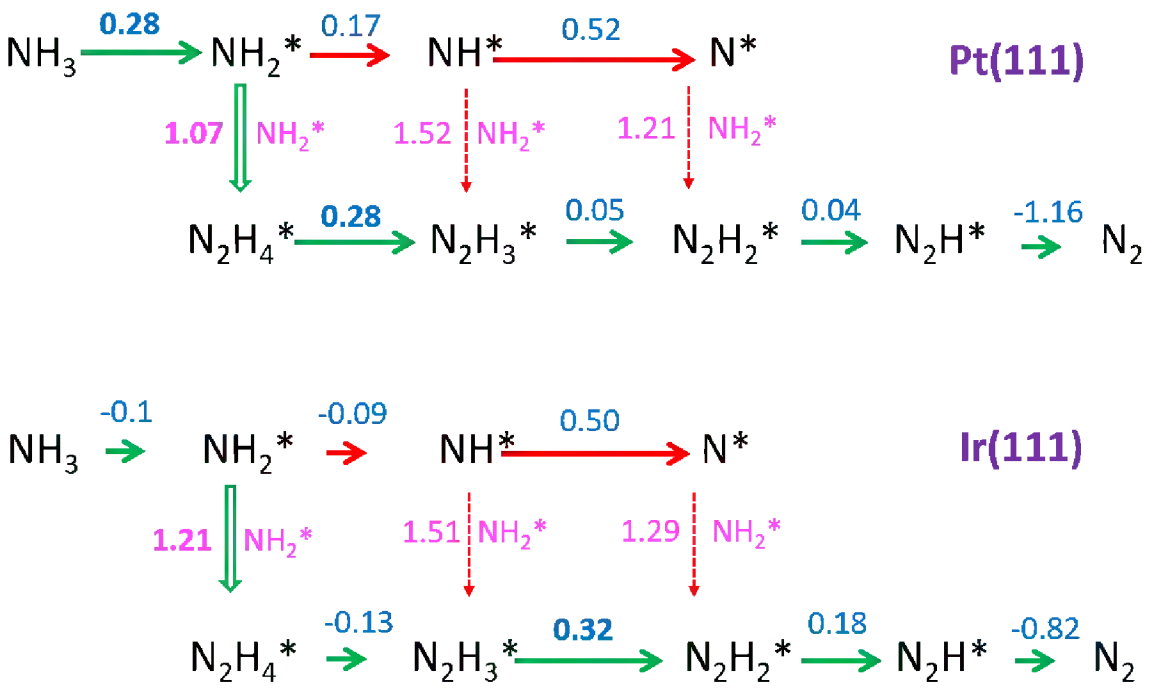

Figure 1. Three reaction pathways for AOR having the lowest activation barriers for dimerization based on the DFT calculations for Pt(111) and Ir(111) surfaces.[23] The green arrows indicate the active pathway via dimerization of two NH_2* and the red horizontal arrows point to the formation of inactive NH* and N* intermediate. The reaction free energies for the 1e deprotonation steps, ΔG, are given in blue above solid arrows and the activation energies for 0e dimerization steps, E_a, are in pink at the side of downward arrows. All in unit of eV. In the deprotonation step from HN_2H_2* to N_2H_2* or HN_2H*, the values given are the smaller ones that are to N_2H_2.[23]

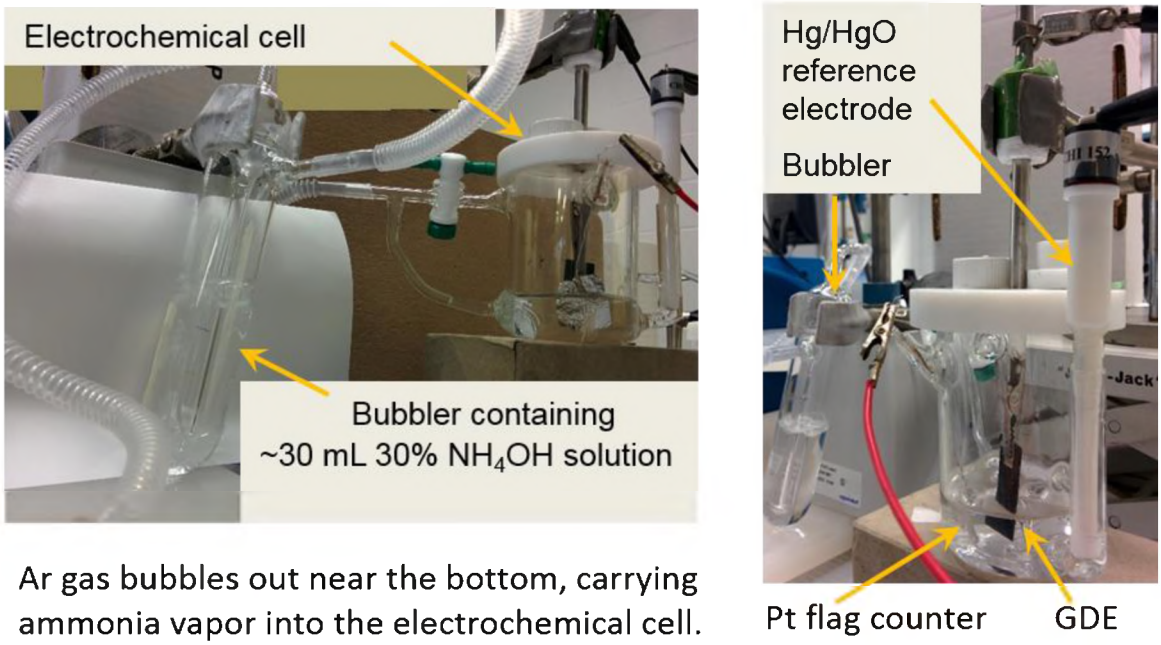

Figure 2. Photos of the bubbler and electrochemical cell used for measuring AOR polarization curves. Ammonia concentrations in the cell are kept at saturation with ammonia partial pressure in the Ar-NH_3 mixed gas at the cell temperatures. The electrochemical cell is in a water bath with a temperature controller during measurements, which is not included in the photo.

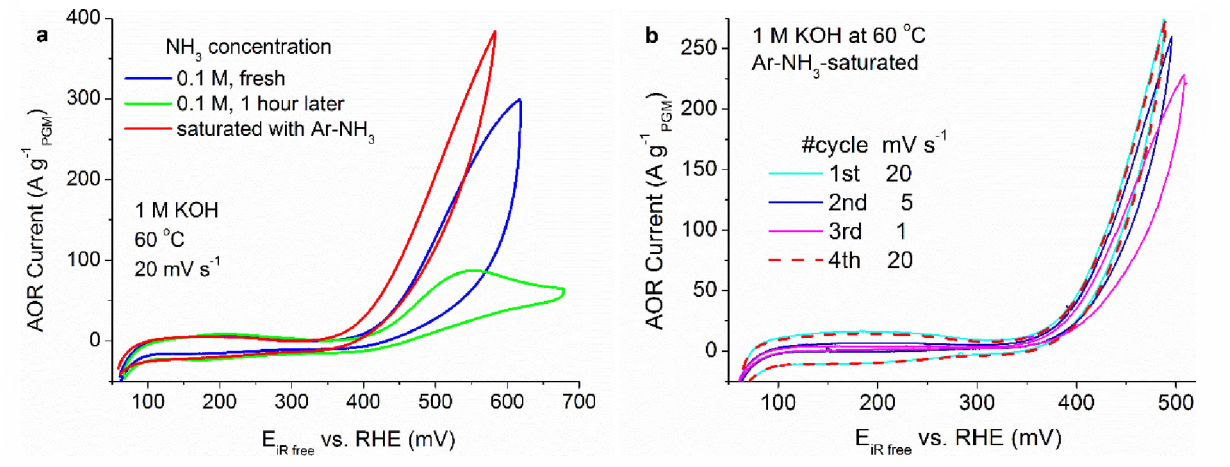

Figure 3. AOR polarization curves for PtIr/C on GDE in 1 M KOH at 60℃. (a) Measured shortly after the solution containing 0.1 M NH_3 was deaerated with Ar gas (blue), about 1 h later (green), and after feeding Ar-NH_3-vaper gas (red). (b) Repeated AOR polarization cycles measured in Ar-NH_3-vapor-saturated 1 M KOH.

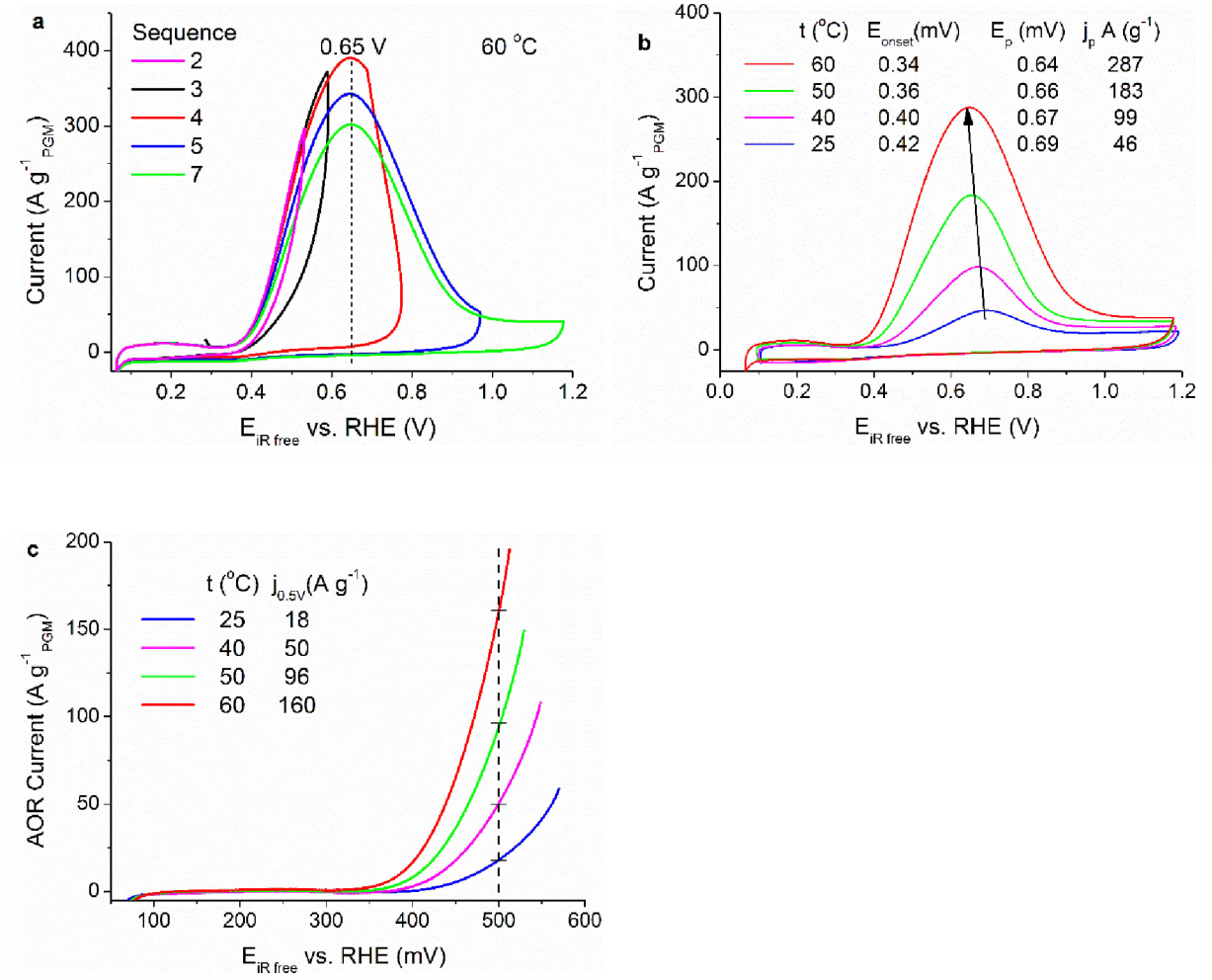

Figure 4. AOR polarization curves for PtIr/C in Ar-NH_3-vapor-saturated 1 M KOH at 20 mV s^{-1}. (a) Measured at 60 °C with increasing high potential limits. (b) The last potential cycle taken at each temperature measured with temperature increased from 25 to 60 °C. (c) The averaged current of positive and negative potential sweeps with 0.6 V potential limit at different temperatures.

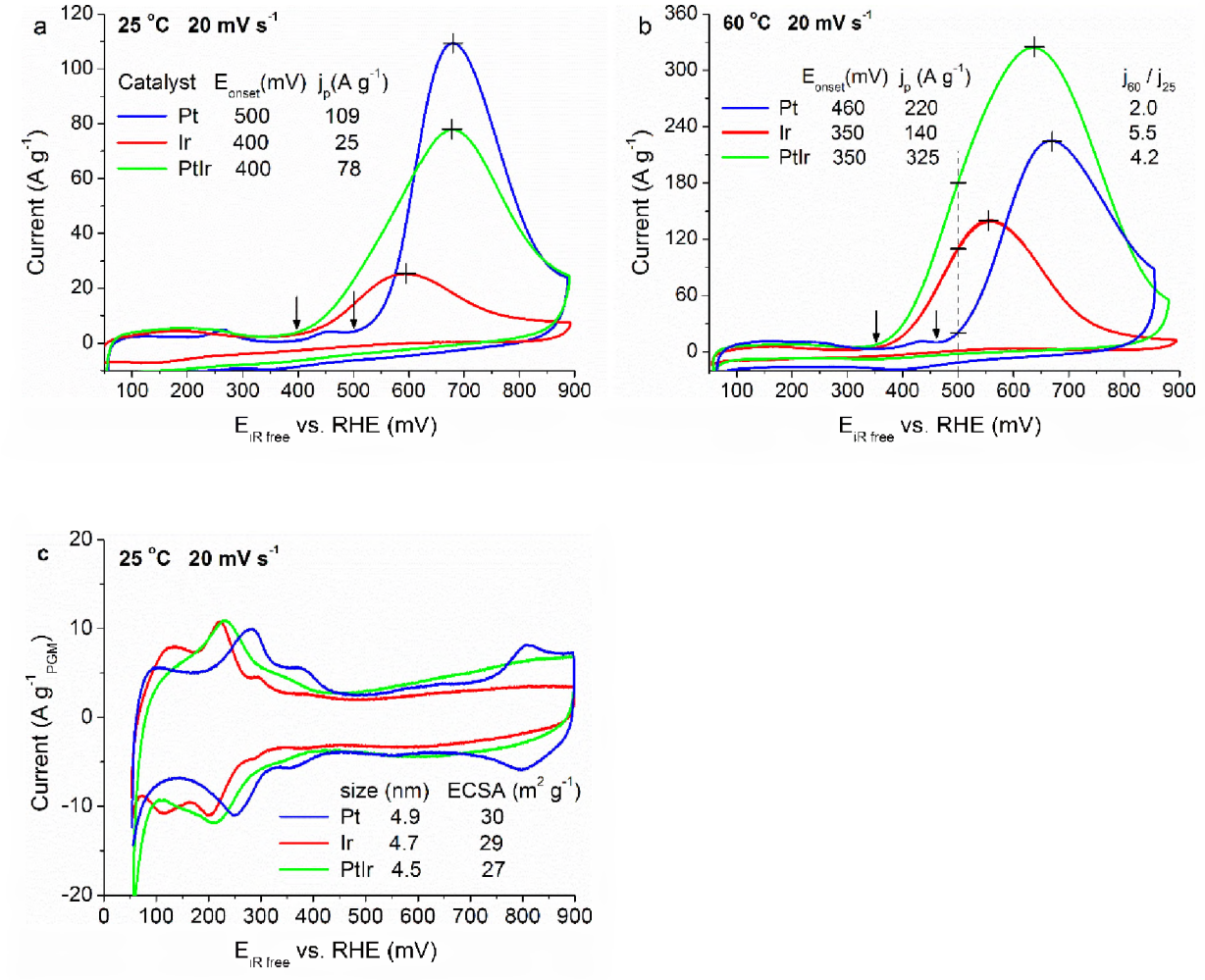

Figure 5. AOR polarization curves for Pt/C, Ir/C, and PtIr/C in Ar-NH_3-vapor-saturated 1 M KOH measured at 25 °C (a) and 60 °C (b), and corresponding voltammetry curves in the absence of ammonia (c). Average particle sizes were determined by XRD and electrochemical surface areas (ECSA) were estimated from integrated charges for hydrogen desorption.

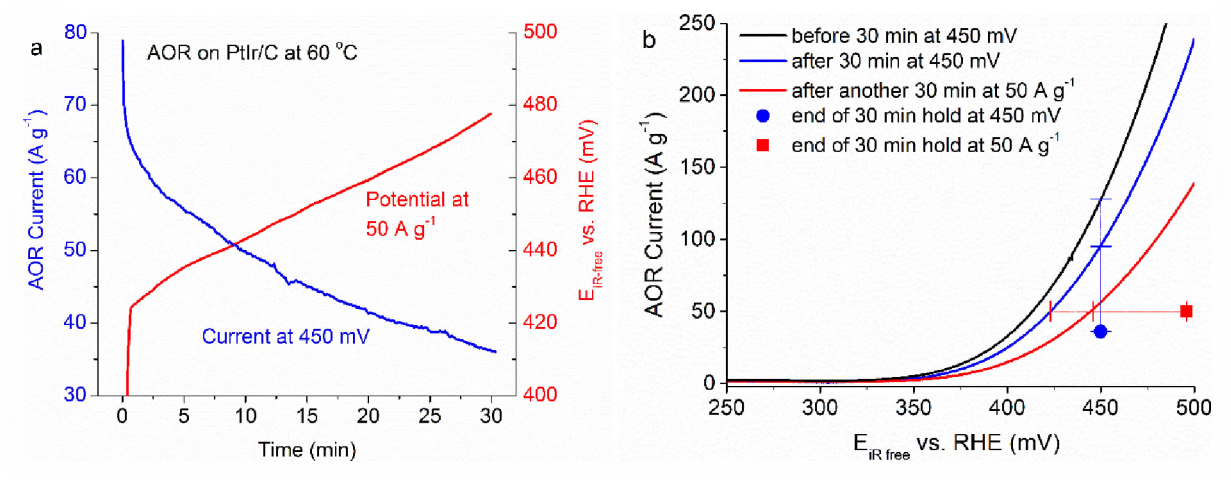

Figure 6. (a) Chronoamperometry (blue, left axis) and chrono potentiometry (red, right axis) curves measured for AOR on PtIr/C in 1 M KOH solution saturated with Ar-NH_3-vapor. (b) AOR polarization curves obtained by averaging the currents in the positive and negative potential sweeps measured at 20 mV s^{-1} before, between, and after chronoamperometry and chronopotentiometry measurements.